Colloids and Surfaces A: Physicochemical and Engineering Aspects 664 (2023) 131155

Contents lists available at ScienceDirect

Colloids and Surfaces A: Physicochemical and Engineering Aspects

journal homepage: www.elsevier.com/locate/colsurfa

Optimized multilayer coating using layer-by-layer assembly method for excellent oxygen barrier of poly(lactic acid) based film

Tina Gulin-Sarfraz [a,*], Magnhild Seim Grøvlen [a], Emil Rosqvist [b], Marit Kvalvåg Pettersen [a], Jouko Peltonen [b], Jawad Sarfraz [a,*]

[a] Nofima, Norwegian Institute of Food, Fisheries and Aquaculture Research, P.O. Box 210, NO-1431 Ås, Norway
[b] Physical Chemistry, Laboratory of Molecular Science and Engineering, Åbo Akademi University, Henriksgatan 2, FI-20500 Åbo, Finland

HIGHLIGHTS

- Greatly improved oxygen barrier properties of a poly(lactic acid) based material.
- Surface evaluations on nano- and microscale reveal a uniform barrier coating.
- The optimized coating has a superior adhesion strength.

GRAPHICAL ABSTRACT

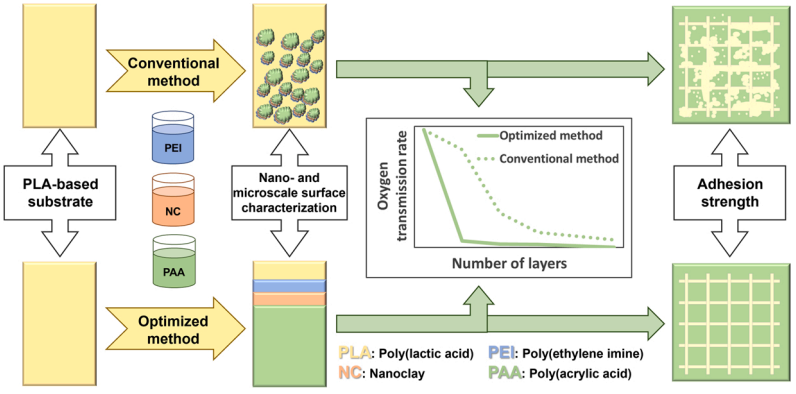

ARTICLE INFO

Keywords:
Polylactic acid
Polyelectrolytes
Nanoclay
Barrier coating
Oxygen transmission rate
Adhesion strength

ABSTRACT

Layer-by-layer assembly (LbL) of trilayer coatings of polyelectrolytes and nanoclays (NC) were produced on poly (lactic acid) based (PLAb) films. The focus of this study was on the optimization of the wetting properties of the PLAb substrate, and the adhesion properties of the prepared coating. Coatings produced by an optimized method, by combining UVC-treatment of the substrate and adjusting surface tension of the coating solutions, were compared to coatings made by typically used water-based solutions. Even though LbL-coatings with a high adhesion strength to its substrate is of outmost importance for most applications, this is often not evaluated. In this study, the adhesion of the coatings on the PLAb substrate was assessed using the cross-cut test according to ISO 2409, in which the adhesion is classified on a scale between 0 and 5, where a lower number reflects better adhesion. The coating prepared by the optimized procedure was categorized as class 0, while the control film was classified as 4. These results reveal the importance of the optimization of both the surface free energy of the substrate, and the surface tension of the dipping solutions. The surface morphology and roughness properties of the optimized films were further investigated with scanning electron microscopy (SEM), confocal optical microscopy (COM) and atomic force microscopy (AFM), showing a uniform distribution of NC on the substrate with increasing number of trilayers. X-ray photoelectron spectroscopy (XPS) confirmed the homogenous surface

* Corresponding authors.
E-mail addresses: tina.gulin-sarfraz@nofima.no (T. Gulin-Sarfraz), jawad.sarfraz@nofima.no (J. Sarfraz).

https://doi.org/10.1016/j.colsurfa.2023.131155
Received 23 December 2022; Received in revised form 15 February 2023; Accepted 17 February 2023
Available online 21 February 2023

composition of polyelectrolytes and NC. Finally, the oxygen transmission rate (OTR) decreased considerably (by 99.7%), from 97.2 cc/(m^2·day) for pristine PLAb substrate to 0.3 cc/(m^2·day) for the 20-trilayer coated substrate.

1. Introduction

One approach to counter the negative environmental impact caused by the petroleum-based polymers used for packaging application is to shift towards more environment friendly biodegradable polymers [1]. Polylactic acid (PLA) is a readily available polymer, it is biodegradable, recyclable, compostable under industrial conditions, and a promising renewable thermoplastic polyester which has the potential to replace the conventional plastic materials [2]. However, the hygroscopic nature, brittleness, and heat sensitivity of PLA makes it less attractive for demanding applications such as food packaging. [3,4] The thermal and mechanical properties are significantly improved in the new commercially available PLA based (PLAb) materials by the addition of copolyester [3]. However, poor oxygen barrier properties limit the application of PLAb for packaging of oxygen sensitive food products [3,5,6]. Oxygen in the packaging environment can, in combination with light exposure at display, lead to pigment oxidation resulting in discoloration in products such as cured meat, sliced salami, etc. [7]. Oxygen may also cause lipid oxidation and rancidity of the products, which limits the shelf life and leads to food waste [8,9]. It is therefore desirable to improve the oxygen barrier properties of PLA-based materials.

Different methods have been reported in the literature for the improvement of the gas barrier properties of the polymers [10]. Among them incorporation of nanofillers in the polymer matrix has been a widely used approach. These nanofillers provide a physical hinderance to the gas molecules and disrupts their diffusion rate by forcing them to adapt tortuous pathways hence positively affecting the gas barrier properties [11]. Different processing techniques including melt extrusion, in situ polymerization and solvent casting has been reported in the literature [10,12–14]. However, the main challenge is to achieve the uniform distribution of the nanofillers in the polymer matrix [15]. Reduction of about 60% in oxygen permeability has been reported in the literature for PLA composites with nanoclays (NC, 5–10 wt%), and at higher concentration aggregation of NC has been reported, resulting in adverse effect on the resulting PLA composite barrier properties [16,17].

In recent years, a layer-by-layer (LbL) deposition method to produce a multilayer film has been reported for the improvement of the barrier properties of different substrates [15]. The underlying principle in the formation of LbL films is the electrostatic interaction between the charged NC and polyelectrolytes. Bi, tri and quadlayer systems have been reported in the literature using NC and different polyelectrolytes [18–21]. LbL assembly consisting of systems such as poly(vinyl alcohol) /montmorillonite (MMT) [22], MMT/chitosan [23], poly(ethylene imine) (PEI)/nanofibrillated cellulose [24], and branched PEI/Nafion/BPEI/MMT [25] has been reported in the literature to improve the oxygen barrier properties of PLA. For MMT based systems the improvement in the gas barrier properties has been mostly linked to exfoliation and orientation of the nanoplates [26].

In this study, we report on a LbL coating consisting of polyelectrolytes and NC on a PLAb substrate to improve the oxygen barrier properties. The coatings were characterized in depth by several surface sensitive techniques to evaluate the distribution of NC on the substrate. The adhesion of the coatings was studied using the cross-cut test, according to ISO 2409. The novelty of this study involves the optimization of the wetting of the PLAb substrate by the solvents (in combination with surface treatment of the substrate), with the resultant decrease in oxygen transmission rate (OTR) values, as well as the notable increase in adhesion of the coating. The overview of the study is schematically described in Fig. 1.

2. Materials and methods

2.1. Materials

Branched poly(ethylene imine) (PEI, average Mw ~25,000), poly (acrylic acid) solution (PAA, average Mw ~100,000, 35 wt% in H_2O)

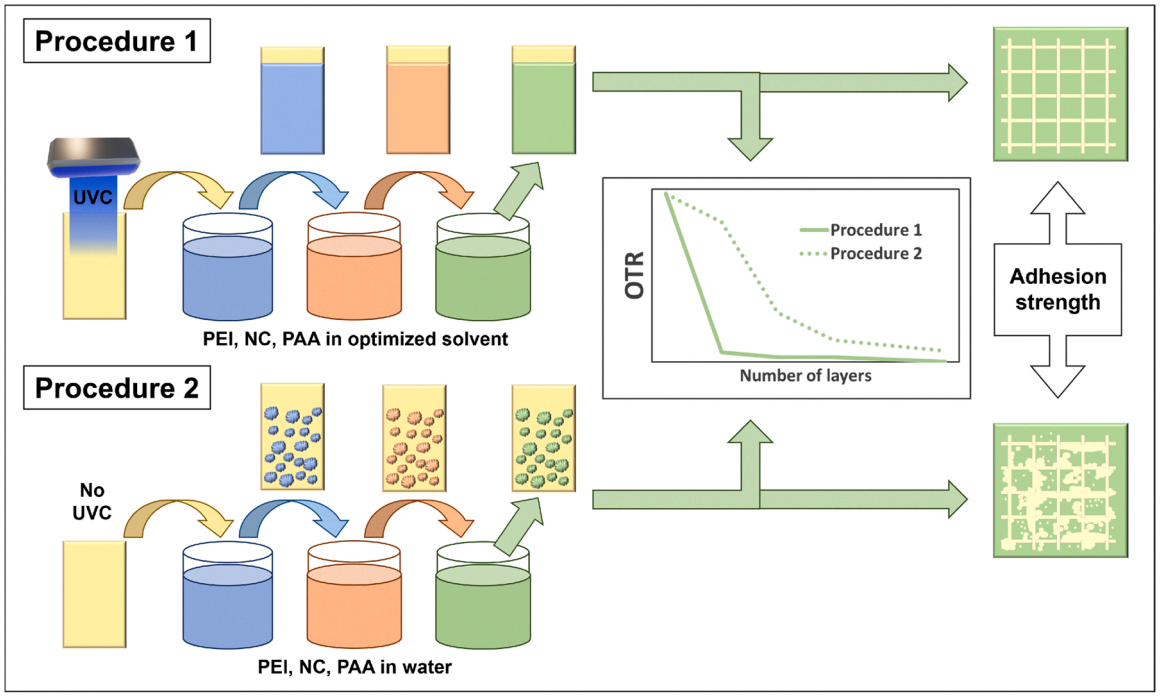

Fig. 1. Schematic overview of the study.

and nanoclay (NC, hydrophilic bentonite) were purchased from Sigma-Aldrich (Merck KGaA, Darmstadt, Germany). Absolute ethanol was obtained from Antibac (Kiilto Oy, Tampere, Finland).

The details about the preparation of the PLA-based film can be found elsewhere [3]. Briefly, commercially available Ecovio® F2224 from BASF was used in this study which is a compound of biodegradable copolyester ecoflex® F Blend and polylactic acid (PLA, NatureWorks®). Films with 300 μm thickness were produced on a blown film extruder model E 25, BL180/400 from Collin Lab & Pilot Solutions GmbH, Germany. The temperature profile on the extruder was set from 160 °C to 183 °C in the different zones, and the extrusion speed was 100 rpm. The die gap was 1.5 mm, and the blow-up ratio was 1:3.

2.2. Solutions and dispersions

The polyelectrolytes PEI and PAA were dissolved in 30 vol% ethanol (for coating procedure 1) or in Milli-Q water (for coating procedure 2). The same solvents were used to disperse the NC. The cationic PEI was dissolved at 0.1 wt%, and further adjusted to pH 10 using 1 M HCl. The anionic PAA was dissolved at 0.2 wt% and adjusted to pH 4 using 1 M NaOH. The NC was dispersed at 1 wt%, by magnetic stirring and ultrasonication.

2.3. Coating preparation

The PLAb substrate was dipped in the following order: PEI, NC, PAA, to complete one single trilayer cycle. The substrate was either untreated (procedure 2) or UVC-treated for 5 min on each side (procedure 1) prior to dipping into the PEI-solution for 2 min using a KSV Nima dip coater (Biolin Scientific Oy, Finland) with dip and drag speed of 100 mm/min. The UVC-treatment of the films were done under ambient conditions at a light intensity of 10 mW/cm^3, using a UVC compact fixture lamp from BÄRO GmbH & Co. KG, Germany. After the first dipping, the substrate was dried in ambient conditions for 5 min and further dipped into the NC-dispersion. When fully immersed, the substrate was immediately pulled with the same drag speed of 100 mm/min. The substrate was again dried for approximately 5 min prior to the dipping in PAA-solution following the same procedure. After this step the coated substrate was dried for 5–8 min, with subsequent UVC-treatment (5 min on each side) for the substrate which followed procedure 1. After this single trilayer coating cycle, the same protocol was continued to produce films with 4, 8, 12, and 20 trilayers. However, only for the first trilayer, the substrate was left in the PEI-solution for 2 min.

2.4. Contact angle measurements

The contact angle measurements were performed using a Theta Lite instrument (Biolin Scientific Oy, Finland). A drop volume of 5 μL was deposited on the substrate and the contact angle was observed over time. Equilibrium contact angle values were acquired when the drop volume, shape and the contact angle remained the same.

2.5. Oxygen transmission rate (OTR)

OTR for the films of pristine and coated PLAb samples was measured with a Dualperm 8001 instrument (Industrial Physics, USA) following the ASTM 3985 standard. The OTR (cc/(m^2·day)) was measured at 23 °C and 50% relative humidity (RH). The testing area of the samples was 5 cm^2. Two parallels were measured.

2.6. Cross-cut test

The adhesion of the coating to the substrate was evaluated according to the ISO 2409 standard. A lattice pattern was cut into the coating using a cross-cut tool (Byk-instruments, Germany), making six parallel cuts (at 1 mm spacing) followed by six perpendicular cuts. A piece of standardized tape (following the cross-cut tool) was placed over the lattice pattern, parallel to one set of cuts, and smoothed over firmly with a finger several times to ensure good adhesion between the tape and the coating. The tape was manually pulled off in a single smooth action at an angle of approximately 60° to the surface. The cross-cut pattern was then studied with a microscope to evaluate the coating adhesion. For each film the test was repeated four times and the results were assessed by comparing the pattern to the ISO 2409 standard classification, class 0–5, as follows: 0 = the lattice is unaffected, none of the squares of the lattice is detached; 1 = detachment of small flakes at the intersection of the cuts, less than 5% of the area is affected; 2 = flaked along the intersection of the cuts with an affected cross-cut area of 5–15%; 3 = squares are partly or wholly damaged, with a cross-cut area of 15–35% being affected; 4 = squares are partly or wholly detached with an affected cross-cut area of 35–65%; 5 = any degree of flaking that cannot be classified under ISO class 4, and has an affected cross-cut area of more than 65%. Thus, a higher number reflects poorer adhesion between the coating and the substrate.

2.7. Coating thickness

The coating thickness was measured using a film thickness gauge (model 543, Qualitest, USA). The measurements were repeated at three different spots.

2.8. Scanning electron microscopy

Thin films produced by the LbL assembly method were characterized for surface morphology by scanning electron microscopy (SEM). SEM imaging was performed with a Zeiss EVO 50 microscope (Carl Zeiss, Cambridge, UK). Prior to the imaging the films were placed on a carbon tape and further sputter coated with gold-palladium alloy with a Polaron SC 7640 sputter coater (Quorum Technologies Ltd, East Sussex, UK).

2.9. Confocal Optical Microscopy

The surface morphology of the films was also investigated by Confocal Optical Microscopy (COM). The COM measurements were carried out with a NanoFocus μSurf 3D white light microscope (NanoFocus AG, Germany). Images were taken with two objectives, at 20x and 50x magnification, giving imaged areas of 800 μm x 772 μm respectively 320 μm x 308.8 μm. All images were taken at a resolution of 512 × 512 pixels. Imaging spots were randomly selected.

2.10. Atomic force microscopy

Atomic force microscopy (AFM) images of 5 μm x 5 μm (512 × 512 pixels) were taken with a Bruker Multimode 8 in PeakForce™ mode. NSG30 cantilevers (spring constant k = 22–200 N/m) were used (NT-MDST, Apeldoorn, Netherlands). Image analysis was done with a MountainSPIP software (v9.2.9994, DigitalSurf, Besançon, France).

The used roughness parameters were as follows: S_q, i.e. the RMS deviation to the mean level of the surface, S_{dr}, the relative increase in surface area due to topography, S_{al}, the distance over which the auto-correlation function decreases to 20%, S_{sk}, skewness, which describes if the surface is peak ($S_{sk}>0$) or valley ($S_{sk}<0$) dominated based on its distribution of heights, S_{ds}, the number of asperities per μm^2 separated by pixels at a lower height level, and S_z, the height between the highest peak and the deepest valley. The error shown is the 95% confidence interval of the roughness data. It was calculated with Microsoft® Excel® 2016 (v.16.0.5356.1000).

2.11. X-ray photoelectron spectroscopy

X-ray photoelectron spectroscopy (XPS) spectra were obtained with a Kratos Axis Ultra^{DLD} XPS instrument using a monochromatic Al Kα X-ray

source (1486.6 eV) with the X-ray source operating at 15 kV and 10 mA at normal emission angle. For survey spectra, 80 eV pass energy was used. XPS measurements were performed on two separate spots for each sample. The atomic concentration (at%) of the different elements was obtained by calculating the area of the peaks and correcting for the sensitivity factors using CasaXPS software.

3. Results and discussion

3.1. Preparation and optimization of the coatings

For LbL assembly, aqueous systems are often reported in the literature [18–21]. Typically, aqueous solutions of polyelectrolytes and NC are used [19–21]. The aqueous system helps to achieve exfoliation of the NC [27]. However, aqueous solutions do not wet plastic substrates very well. In our case, the equilibrium water contact angle on pristine PLAb substrate was 102º, which indicates a relatively poor wetting of the substrate. Previously, UVC-treatment has been demonstrated to reduce the water contact angle values and improve the adhesion by increasing the bond strength between a substrate and the coating material. [28,29] Thus, the PLAb substrate was treated with UVC for 1, 5 and 10 min and the water wettability of the substrate improved with equilibrium water contact angles decreasing to 88º, 80º and 79º, respectively. To further improve the wetting of the PLAb substrate, the surface tension of water was decreased with the addition of ethanol. The surface tension values of 72, 56.2, 47.8 and 41.6 mN/m for pure water, 10%, 20% and 30% ethanol, respectively, are reported in the literature at 25 ℃ [30]. Mixed solvents with different ratios of water and ethanol were prepared and their contact angles were measured on the PLAb substrate (Table 1). As expected, a significant drop in contact angle values were observed, from 102º for water to 80º for 30% ethanol. Similarly, the contact angle values for PEI also dropped when the solution was made in 30% ethanol compared to water only (Table 1). Further, the combined effect of UVC-treatment and mixed ethanol-water solvent was studied on the wettability of the PLAb substrate. The contact angle of only 58º was measured after 10 min of UVC-treatment with 30% ethanol in water. After these optimization steps, multilayered films of polyelectrolytes and NC were deposited on the PLAb substrate using the LbL assembly approach. For comparison purposes, the films were deposited on the PLAb substrate using two separate procedures. In procedure 1, the PLAb substrate was treated with UVC and the surface tension of the dipping solutions was decreased by using mixed solvents of water and ethanol (30%). For procedure 2, untreated PLAb substrate was used in combination with aqueous solutions. The two different procedures are schematically described in Fig. 1.

3.2. Oxygen barrier properties and morphology of the coatings

The oxygen barrier properties were measured and related to the morphology of the films, as visualized with optical microscopy. Fig. 2 shows the oxygen transmission rate (OTR) values of the films produced by procedure 1 and 2. In addition, the OTR values are reported in Supplementary Table ST1. While 4, 8, 12 and 20-trilayer films show a reduction of 17%, 70%, 87% and 93% in the OTR values compared to pristine PLAb when produced by procedure 2, the % reduction in the OTR value for trilayer films produced by procedure 1 was more pronounced and the values of 94%, 97%, 97% and 99.7% were obtained. The OTR value for the 20-trilayer film is 0.3 cc/(m^2·day) which can be classified as a high oxygen barrier coating. A typical value of a high oxygen barrier coating for food packaging applications is below 1 cc/(m^2·day), where for example 1 mm thick polyethylene terephthalate (PET) is in the range of 1.2–2.4 cc/(m^2·day) [31]. Further evaluation of the 20-trilayer films produced by the two different methods reveal that the optimized film has a more uniform and compact surface structure than the control film, as presented by microscopy images in Fig. 3. As expected, on microscale the coating on the control film is formed as patches due to the lack of adhesion between the coating and the substrate (Fig. 3b).

Table 1
Equilibrium contact angle (CA_{eq}) of water/ethanol mixtures, and of PEI dissolved in water/ethanol, on PLAb substrate. Comparison of untreated and UVC-treated samples.

Water: Ethanol	CA_{eq}	CA_{eq} after 10 min UVC-treatment	CA_{eq} of 0.1% PEI	CA_{eq} of 0.1% PEI after 10 min UVC-treatment
10:0	102º	79º	99º	76º
9:1	93º	74º	94º	75º
8:2	84º	69º	82º	64º
7:3	80º	63º	72º	58º

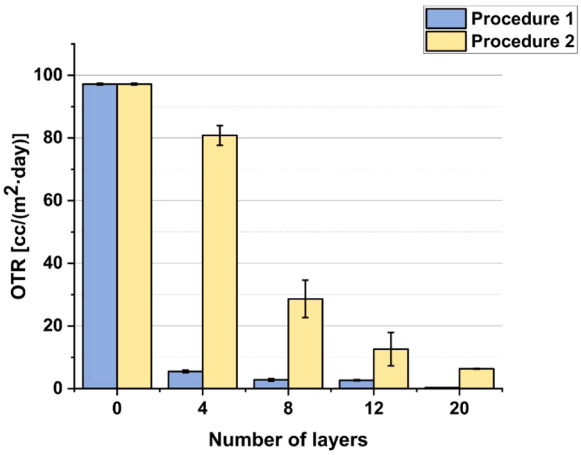

Fig. 2. Oxygen transmission rates (OTR), at 23 °C and 50% RH, for the trilayer coatings prepared by the two different procedures (1 and 2) as a function of the number of trilayers. The shown error is the standard deviation.

In the literature, the improvement in the gas barrier properties using LbL assembly has been explained by the formation of brick wall structure [19–21]. This structure is produced when the substrate is evenly covered by the NC platelets. The deposited NC provides a physical hinderance towards the diffusion of the gas molecules. With the brick wall structure, the gas molecules are compelled to adopt a tortuous path, which significantly decreases their diffusion rate hence improving the gas barrier properties [15]. The formation of a homogeneous structure is therefore critical for the improvement in the gas barrier properties. The bentonite NC used in this study has a high swelling capacity [32], and thus forming a large surface area in solution. In dry state, prior to exfoliation, the sheets form sphere-like aggregates (Supplementary Figure SF1). Prior to the deposition of the NC on the PLAb-substrate, the NC-suspension was treated with ultrasonication to disperse the NC platelets and improve the NC exfoliation. As presented in Fig. 2, the reported method in this paper is promising for the improvement of the gas barrier properties of hydrophobic plastic substrates. Interestingly, even though the water-based coatings (procedure 2) form patches on the PLAb-substrate (Fig. 3), the OTR-value can be greatly improved with increasing number of layers (Fig. 2).

3.3. Adhesion test of the coatings

Coating with a good adhesion strength to its substrate is of fundamental importance for most applications. However, this has mostly been neglected in published studies related to LbL coatings. Here, the adhesion of the LbL coatings on the PLAb substrate was evaluated using the cross-cut test, according to the ISO 2409 standard. In this test the coatings are classified on a scale between 0 and 5, by comparing the cross-cut pattern to the standard classification, where a higher number reflects poorer adhesion between the coating and the substrate. The

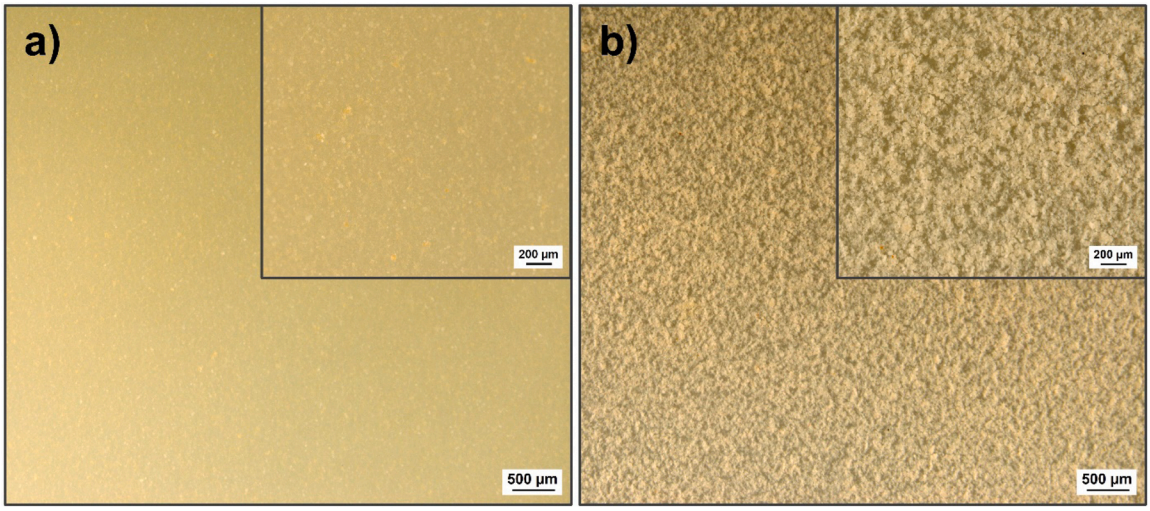

Fig. 3. Optical microscopy images of PLAb films coated with 20 trilayers according to (a) procedure 1 and (b) procedure 2. The insets show zoomed images.

cross-cut test was performed on the 20-trilayer films produced by both methods, procedure 1 and 2. During the cross-cut test the films were analyzed with optical microscopy to assure high-resolution images and thus precise evaluation. Representative images are shown in Fig. 4. The PLAb-substrate coated according to procedure 1 showed a very good adhesion in the cross-cut test, where the lattice pattern is completely unaffected, resulting in a class 0 classification. Contrary, the coating made by procedure 2 showed a very poor adhesion rate (Fig. 4b). For each film the test was repeated four times (Supplementary Figure SF2) and the results were assessed based on an average of the tests. The coating prepared by procedure 2 was categorized as class 4, since large parts of the cross-cut area was damaged due to the weak adhesion. The coating had flaked along all the edges of the cuts and some squares were partly detached from the substrate. These results point to the fact that the pre-treatment of the substrate, as well as the optimization of the surface tension of the solvents, is critical for ensuring good coating adhesion.

3.4. Surface morphology of the optimized films

The microstructure and surface morphology of the films obtained by coating procedure 1 was examined with scanning electron microscopy (SEM), confocal optical microscopy (COM), and atomic force microscopy (AFM). For SEM, various surface sections of the pristine and the 4, 8, 12 and 20-trilayer coated films were imaged to investigate the dispersion quality of NC on the surface. Randomly chosen areas were scanned to investigate possible defects in the coating layer. Representative images at different magnifications are shown in Fig. 5, where Fig. 5a presents the pristine PLAb substrate. Significant differences are observed for the 20-trilayer film compared to the other films. Images at the magnification of 500 show aggregated morphology for the 20-trilayer film (Fig. 5e). These aggregated structures are densely packed and provide uniform coverage of the surface (Fig. 5f). However, for 4, 8, and 12-trilayer films (Fig. 5b–d), the aggregates are relatively smaller in size and are scattered at the surface. In addition, the inset images reveal the sheet-like structure of the NC. It can be further seen that the NC coverage of the PLAb substrate improves with increasing number of trilayers from 4 to 20. Micro-cavities can be seen for the 20-trilayer film, but no cracks were observed. The thickness of the trilayer coatings were approximately 5 µm, 7 µm, 15 µm, and 20 µm for 4, 8, 12 and 20 trilayers, respectively, as evaluated with a film thickness gauge (Supplementary Figure SF3).

The build-up of the first trilayer coating was imaged with COM at the different stages in the coating procedure. Representative images are shown in Supplementary Figure SF4. The roughness average (S_a) and the root mean square roughness (S_q) of the samples were calculated from the

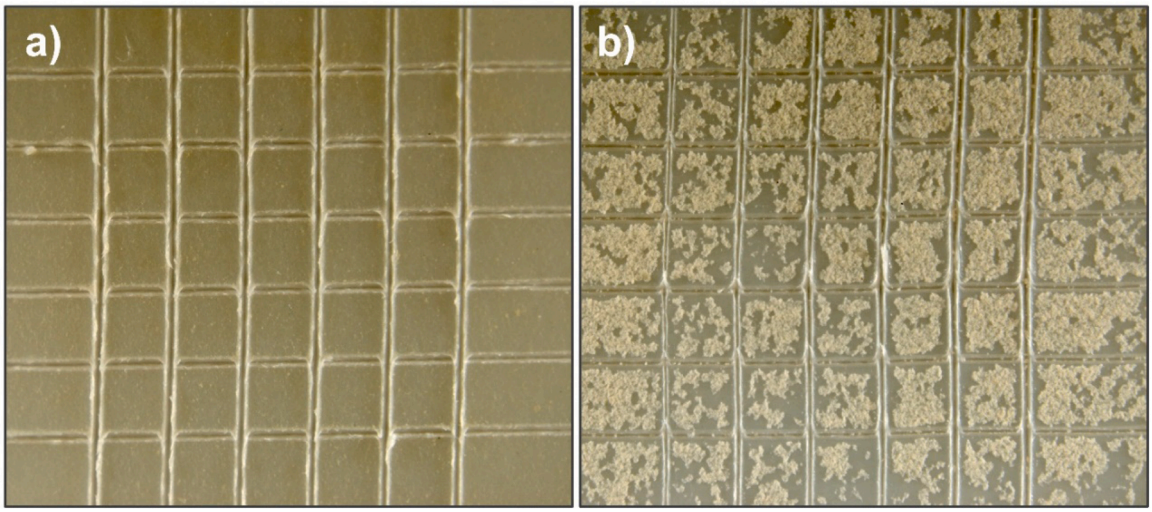

Fig. 4. Representative optical microscopy images of cross-cut areas on 20-trilayer films deposited with (a) procedure 1 and (b) procedure 2.

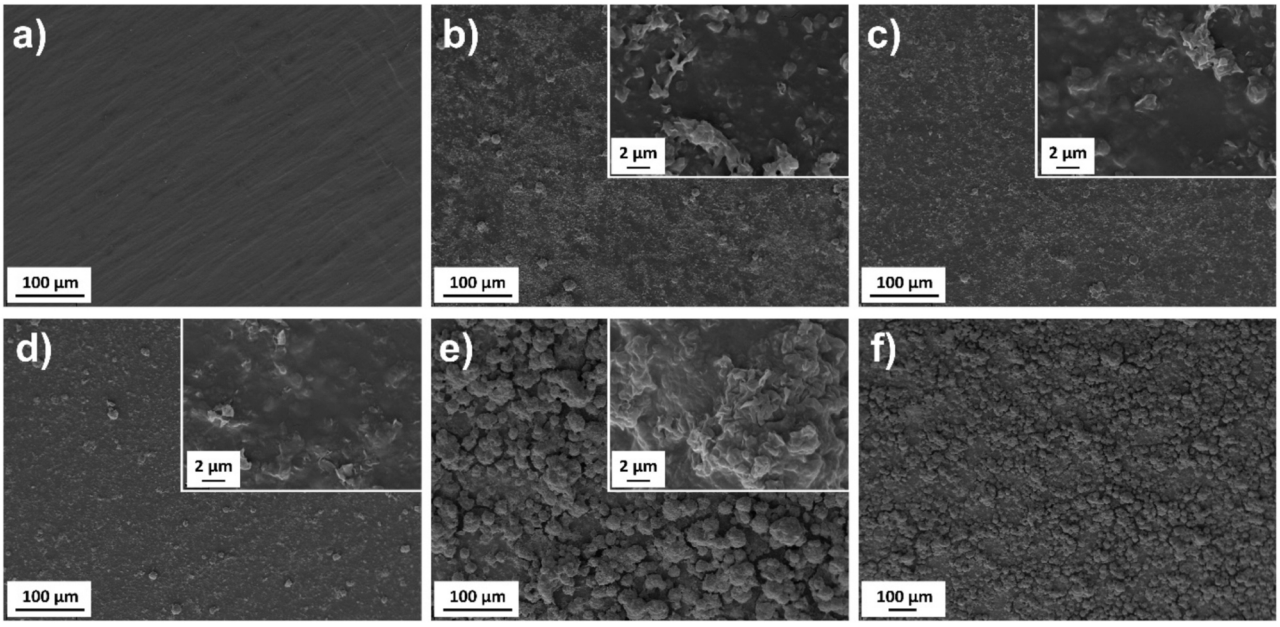

Fig. 5. Scanning electron microscopy images of (a) pristine PLAb substrate and (b) 4, (c) 8, (d) 12 and (e) 20-trilayer films at 500 times magnification with inset images at 15,000 times magnification. The 20-trilayer film is homogenous with no visible cracks, as shown in (f) at lower (200 times) magnification.

COM images at different cutoffs. The calculated values are listed in Supplementary Tables ST2-ST9. Fig. 6 presents the cut-off dependency for the trilayer coating, while the results for the pristine PLAb and the first PEI and PEI/NC coatings are presented in Supplementary Figures SF5–SF6. The results in Fig. 6 show how the S_a roughness of the trilayer coating increases with increasing cut-off. The S_q of the trilayer coating also increases, up to an S_q of approx. 380–400 nm from a cut-off of 200 µm. At the same cut-off, the S_a roughness is slightly lower, 280 nm. It has been shown that sampling interval influences the calculated roughness. The parameters S_q and autocorrelation length have been particularly highlighted, with said parameters increasing in size as growing wavelength features are included in the image analysis. In this case, the plateauing of S_q at 380–400 nm could thus be attributed to the wavelength limit of the surface [33]. Such an analysis shows that the S_q roughness of the PLAb substrate is on a similar level, from COM images at a cutoff of 300 µm, both before and after coating with PEI and PEI/NC (493, 470, and 463 nm, respectively, as shown in Supplementary Figures SF6. The PAA layer smoothens the film to an S_q of 404 nm. The multilayer coatings could unfortunately not be analyzed with COM due to the light absorptive and reflective character of the sample. This was likely due to the increasing amount of NC on the surface.

However, AFM was applied to further analyze the assembly of NC platelets with the polyelectrolytes on a lower length scale. Representative images can be seen in Supplementary Figure SF7, and the calculated roughness values are presented in Fig. 7 and Supplementary Table ST10. The S_q value, indicating height variations, for films without NC was comparatively low and homogenous (as seen by the low error), for pristine PLAb S_q 39 nm and for PLAb with a PEI-layer 19 nm with relative error of approximately 22–36%. The addition of the NC layer increased the roughness significantly, to 94 nm with a relative error of 50%. For completed trilayer coating, the S_q did not change significantly, and it remained around the same level as additional trilayers were added (Fig. 7A). All coatings with NC appeared heterogeneous on this level (5 µm x 5 µm images) with high relative errors due to the height variations. The S_{dr} parameter also showed an increase with the addition of NC to the surface. Addition of a PAA layer or further multilayers did not

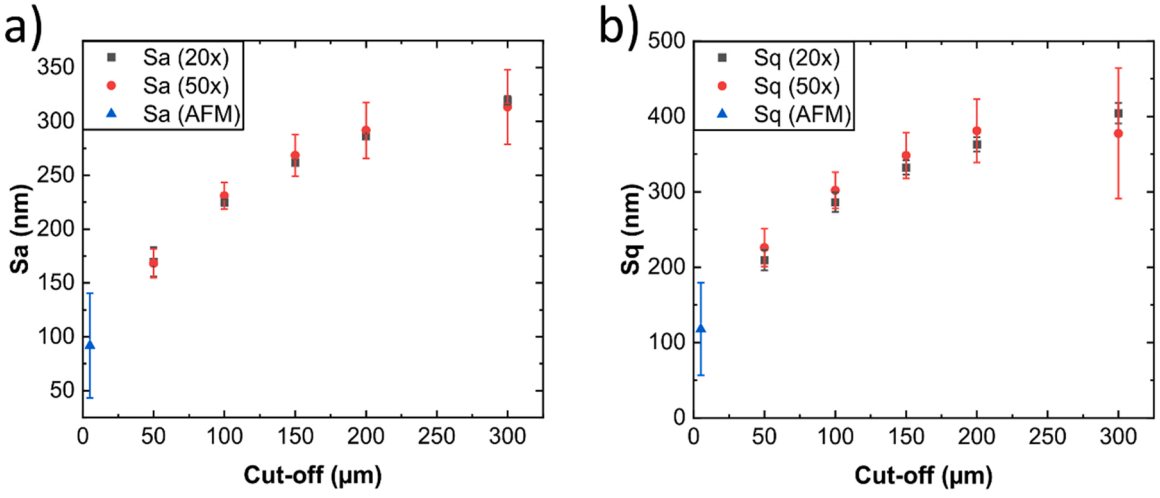

Fig. 6. The cut-off dependency of the S_a and S_q roughness of a single trilayer coating, from COM images at two magnifications, 20x (black) and 50x (red), as well as AFM data (blue), approximating the AFM image size as being equal to cut-off. The shown error is the standard deviation.

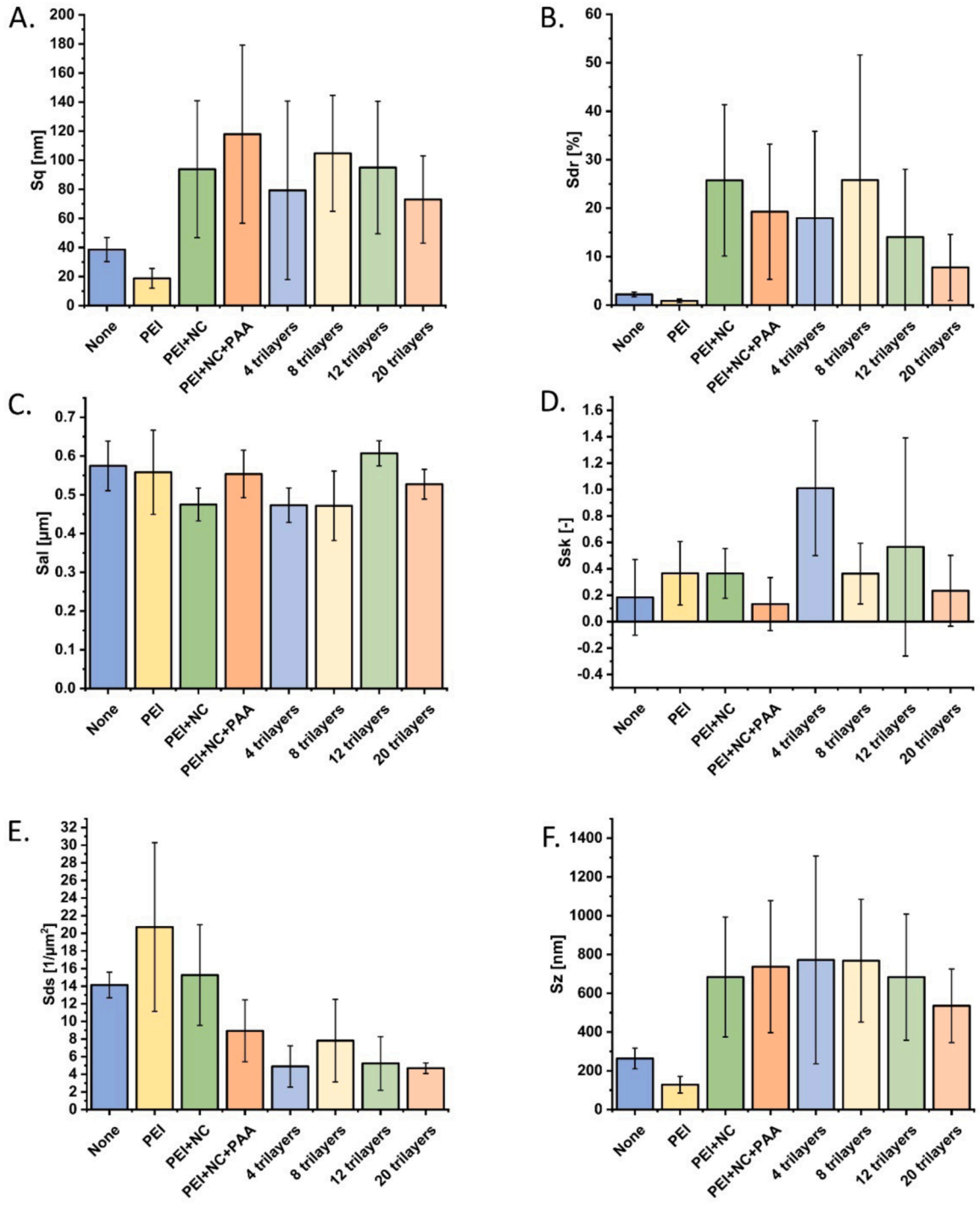

Fig. 7. Surface roughness of the coatings on the PLAb substrate as described by the parameters a) S_q, b) S_{dr}, c) S_{al}, d) S_{sk}, e) S_{ds}, and f) S_z. All parameters were obtained from 5 µm x 5 µm images. The error shown is the 95% confidence level.

change the S_{dr} parameter to a significant level. However, the 20-trilayer film gave rise to a slightly smaller value which in combination with the smaller error for the S_{dr} parameter indicated a more homogenous surface with less relative increase in surface area due to topography (Fig. 7B). The autocorrelation length, S_{al}, which can be used as a measure of lateral roughness, was fairly similar for all surfaces (0.4–0.6 µm, with a relative error typically around 10%), as seen in Fig. 7C. Fig. 7D presents the surface skewness, S_{sk}, which corresponds to the asymmetry degree of the surface heights to the mean plane, i.e., a value of zero indicates a symmetrical surface. The S_{sk} value for the 20 trilayer film is similar to the S_{sk} value for uncoated PLAb, indicating a uniform distribution of the NC. Further, the density of summits, S_{ds}, indicating number of peaks per unit area, was between 14 μm^{-2} and 21 μm^{-2} for the pristine PLAb, PLAb/PEI and PLAb/PEI/NC. From this it decreased to around 5–9 μm^{-2} for coatings with PAA, with a clear decrease in the error for the 20-trilayer film (Fig. 7E). These results can be explained by the relatively uniform distribution of NC, especially for the 20-trilayer film. Additionally, the S_z parameter, which presents the height between the highest peak and the deepest valley, increased from 128 nm for PLAb/PEI to approximately 535–772 nm for the different trilayer samples (Fig. 7F).

These results obtained on the nanoscale are in good agreement with

the microscale analysis acquired by COM and SEM. The datasets obtained by COM and AFM can describe the roughness over a range of length scales from the scale of individual NC platelets (AFM) to the overall roughness of the film (COM), as shown in Fig. 6.

3.5. Evaluation of the surface composition of the optimized films

X-ray photoelectron spectroscopy (XPS) is considered a highly surface sensitive technique in which the elemental composition of solid surfaces can be studied to a depth of about 10 nm [34]. The atomic concentrations of the detected elements at two different spots for each sample is shown in Table 2. XPS measurements were performed on pristine PLAb, PLAb coated with PEI (PLAb/PEI), further coated with NC (PLAb/PEI/NC), and at the completion of the cycle with PAA (PLAb/-PEI/NC/PAA), to study the variation in the surface composition of PLAb upon completion of one trilayer cycle. Furthermore, spots at films with 4, 8, 12 and 20-trilayer cycles were also measured. It can be seen in Table 2 that the atomic concentration of carbon (C) and oxygen (O) for PLAb substrate is very similar for the two separate spots, confirming the uniform composition of the PLAb material. Furthermore, small amounts of silicon (Si) and calcium (Ca) were detected, which might have originated from silica and calcium carbonate, which are commonly used fillers. In addition, the NC is likely to have small impurities of Ca. Negligible amount of sulfur (S) possibly related to contamination is also detected. For PLAb coated with PEI, an increase in the atomic concentration of nitrogen (N) was observed confirming a successful deposition of the PEI-layer (Table 2). However, there is little change in the concentration of N from 4-trilayers to 20-trilayers. Since the detection depth is only around 10 nm, the amount of N is not changing much as additional trilayers are built up. Furthermore, detection of aluminum (Al) and multifold increase in the atomic concentration of Si from the PLAb/PEI/NC samples compared to PLAb and PLAb/PEI samples confirm the presence of NC at the surface. This is in agreement with the literature as Si and Al are the two main components of the bentonite (NC) used in this study [35]. However, a significant variation was observed in the Al, C, O and Si concentrations from the two different spots, which implies that the NC coverage at the surface was not uniform. At the end of the cycle, the PLAb substrate was dipped into anionic PAA. This was done to facilitate the filling of the exposed regions between the NC [20]. These regions are formed where PEI has not interacted with NC. Since the pH of PAA solution is much lower (pH 4), when dipped, the exposed PEI will be at highly charged state, promoting the attraction with PAA. The aim is to have a more uniform negatively charged surface at the end of the trilayer cycle. The effective deposition of PAA at the end of the first cycle was further confirmed. The atomic concentration of N, which is related to PEI, decreased for PLAb/-PEI/NC/PAA sample compared to PLAb/PEI/NC sample as shown in Table 2.

Moreover, the formation of uniform NC structure with increasing trilayer cycles (from 4 to 20) was confirmed with XPS. Substantial variation in the atomic concentration of Al was observed from two separate spots for 4 and 8-trilayer cycles with standard deviation of 0.4 % and 0.7 %, respectively, indicating heterogeneous structures (Table 2). On the other hand, the variation in the atomic concentrations of Al for 20-trilayer cycles was negligible (standard deviation of 0.01 %) suggesting the formation of a more homogeneous structure. The XPS spectra for PLAb substrate and coated substrates can be seen in Supplementary Figures SF8–SF15.

Table 2
Compilation of surface analysis data listing the atomic concentrations of the detected elements (Al: Aluminum, C: Carbon, Ca: Calcium, N: Nitrogen, O: Oxygen, S: Sulfur, Si: Silicon). The two rows for each sample present parallel measurements. PLAb: polylactic acid based material, PEI: poly(ethylene imine), NC: nanoclay, PAA: poly(acrylic acid).

	Al2p %	C1s%	Ca2p %	N1s %	O1s %	S2p %	Si2p %
PLAb		77.4	1.266	0.39	20.1	0.3	0.5
		77.6	0.52	1.1	19.7	0	1.1
PLAb/PEI		80.8	0.67	2.44	14.8	0.16	1.04
		79.5	0.67	2.49	15.9	0	1.38
PLAb/PEI/NC	1.2	72.3	0.98	2	18.9	0.33	4.25
	3.4	54.7	0.96	2.89	27.3	0.1	10.5
PLAb/PEI/NC/ PAA	2.6	60	0.86	1.6	24.8	1.3	8.7
	3.55	56	1.08	1.21	26.2	1.9	10
4 -trilayer	1.6	59.6	0.8	7.44	24.2	0.68	5.6
	2.2	57	0.4	7.8	25.8	0.8	5.8
8-trilayer	1.45	60.4	0.47	8.65	23.5	0.61	4.9
	2.44	55.7	0.59	8.16	25.9	0.36	6.76
12-trilayer	2.25	53.8	0.5	9.1	26.8	0.4	7.1
	2.51	54.54	0.44	8.98	25.9	0.4	7.15
20-trilayer	1.8	56	0.5	8.6	28	0.3	5.2
	1.82	55	0.5	8.9	27.4	0.5	5

4. Conclusions

In this paper we reported an improved method for the deposition of NC and polyelectrolytes on a PLAb substrate using LbL assembly. The substrate was treated with UVC to improve the surface free energy, and the surface tension of the dipping solutions was reduced by mixing ethanol with water. The good wetting of the dipping solutions with the UVC-treated substrate was confirmed with contact angle measurements, where an equilibrium contact angle of 58° was measured. The resulted films had uniform surface structure as compared to the films produced by dipping the substrate in the aqueous solutions, and the adhesion between the coating and the substrate was greatly improved. The XPS results confirmed the successful deposition of polyelectrolytes and NC. Furthermore, XPS results showed very low standard deviation in the atomic concentration of the detected elements at the substrate surface after 20-trilayer cycles, confirming the formation of homogeneous structures. SEM further confirmed that the 20-trilayer film produced with the modified method was uniform. No cracks or pinholes were observed. In addition, AFM analysis revealed a relatively homogeneous surface of the 20-trilayer film even on the nanoscale. The coating produced by the optimized method led to a substantial improvement of the oxygen barrier properties of the PLAb substrate, as confirmed with OTR measurements. This is a proof-of-concept study, showing that uniform NC structures with good adhesion strength can be produced on hydrophobic substrates by surface treatment of the substrate and optimization of surface tension of the dipping solution. However, the process presented here is laborious. In the future studies, we will explore the possibility of utilizing easily up-scalable methods to improve the gas barrier properties of environment-friendly green packaging materials.

Funding

This work was supported by Nofima (project PackTech, grant number 12596); Research Council of Norway (project NanoFunPack, grant number 302243); Norwegian Fund for Research Fees for Agricultural Products, FFL (project Future Food Control, grant number 314743); and Jane and Aatos Erkko foundation (project ABC-Health).

CRediT authorship contribution statement

Tina Gulin-Sarfraz: Conceptualization, Investigation, Methodology, Validation, Visualization, Writing – original draft, Writing – review & editing. **Magnhild Seim Grøvlen**: Investigation, Writing – review & editing. **Emil Rosqvist:** Investigation, Methodology, Validation, Visualization, Writing – review & editing. **Marit Kvalvåg Pettersen:** Writing – review & editing. **Jouko Peltonen**: Methodology, Resources, Validation, Writing – review & editing. **Jawad Sarfraz:** Conceptualization, Funding acquisition, Investigation, Methodology, Project administration, Resources, Supervision, Validation, Visualization, Writing –

original draft, Writing – review & editing.

Declaration of Competing Interest

The authors declare that they have no known competing financial interests or personal relationships that could have appeared to influence the work reported in this paper.

Data Availability

Data will be made available on request.

Acknowledgements

Jorunn Nilsen at Norner AS is acknowledged for assisting in selection and producing the PLA-based film substrate for this study. Hilde Raanaas Kolstad at Imaging Centre, Norwegian University of Life Sciences (NMBU), is acknowledged for technical assistance with SEM imaging.

Appendix A. Supporting information

Supplementary data associated with this article can be found in the online version at doi:10.1016/j.colsurfa.2023.131155.

References

[1] T. Zhang, Q. Yu, L. Fang, J. Wang, T. Wu, P. Song, All-organic multilayer coatings for advanced poly (lactic acid) films with high oxygen barrier and excellent antifogging properties, ACS Appl. Polym. Mater. 1 (12) (2019) 3470–3476.
[2] J. Nilsen-Nygaard, E.N. Fernández, T. Radusin, B.T. Rotabakk, J. Sarfraz, N. Sharmin, et al., Current status of biobased and biodegradable food packaging materials: Impact on food quality and effect of innovative processing technologies, Compr. Rev. Food Sci. Food Saf. 20 (2) (2021), 1333-80.
[3] J. Sarfraz, A.Å. Hansen, J.-E. Haugen, T.-A. Le, J. Nilsen, J. Skaret, et al., Biodegradable active packaging as an alternative to conventional packaging: a case study with chicken fillets, Foods 10 (5) (2021) 1126.
[4] V. Sangeetha, H. Deka, T. Varghese, S. Nayak, State of the art and future prospectives of poly (lactic acid) based blends and composites, Polym. Compos. 39 (2018) 81–101.
[5] J. Wang, D.J. Gardner, N.M. Stark, D.W. Bousfield, M. Tajvidi, Z. Cai, Moisture and oxygen barrier properties of cellulose nanomaterial-based films, ACS Sustain. Chem. Eng. 6 (1) (2018) 49–70.
[6] S. Singha, M.S. Hedenqvist, A review on barrier properties of poly (lactic acid)/clay nanocomposites, Polymers 12 (5) (2020) 1095.
[7] O. Sørheim, I. Måge, H. Larsen, Determination of critical levels of residual oxygen to minimize discoloration of sliced packaged Norwegian salami under light display, Meat Sci. 129 (2017) 88–92.
[8] A.K. Pal, V. Katiyar, Nanoamphiphilic chitosan dispersed poly(lactic acid) bionanocomposite films with improved thermal, mechanical, and gas barrier properties, Biomacromolecules 17 (8) (2016) 2603–2618.
[9] V.K. Haugaard, A.M. Udsen, G. Mortensen, L. Høegh, K. Petersen, F. Monahan, Potential food applications of biobased materials. An EU-concerted action project, Starch-Stärke 53 (5) (2001) 189–200.
[10] Y. Cui, S. Kumar, B.R. Kona, D. van Houcke, Gas barrier properties of polymer/clay nanocomposites, RSC Adv. 5 (78) (2015), 63669-90.
[11] L.E. Nielsen, Models for the permeability of filled polymer systems, J. Macromol. Sci. Chem. 1 (1967) 929–942.
[12] J.H. Chang, Y.U. An, G.S. Sur, Poly (lactic acid) nanocomposites with various organoclays. I. Thermomechanical properties, morphology, and gas permeability, J. Polym. Sci. Part B: Polym. Phys. 41 (1) (2003) 94–103.
[13] S.R. Chowdhury, Some important aspects in designing high molecular weight poly (l-lactic acid)–clay nanocomposites with desired properties, Polym. Int. 57 (12) (2008), 1326-32.
[14] H.S. Na, S.C. Kim, Effect of Organoclays on silicate layer structures and thermal stabilities of in-situ polymerized poly (D-lactide)/clay nanocomposites, J. Macromol. Science®, Part A: Pure Appl. Chem. 47 (3) (2010) 254–264.
[15] J. Sarfraz, T. Gulin-Sarfraz, J. Nilsen-Nygaard, M.K. Pettersen, Nanocomposites for food packaging applications: an overview, Nanomaterials 11 (1) (2021) 10.
[16] J.-W. Rhim, S.-I. Hong, C.-S. Ha, Tensile, water vapor barrier and antimicrobial properties of PLA/nanoclay composite films, LWT-Food Sci. Technol. 42 (2) (2009) 612–617.
[17] S.S. Ray, M. Okamoto, Polymer/layered silicate nanocomposites: a review from preparation to processing, Prog. Polym. Sci. 28 (11) (2003), 1539-641.
[18] W.-S. Jang, I. Rawson, J.C. Grunlan, Layer-by-layer assembly of thin film oxygen barrier, Thin Solid Film. 516 (2008) 4819–4825.
[19] M.A. Priolo, D. Gamboa, J.C. Grunlan, Transparent clay− polymer nano brick wall assemblies with tailorable oxygen barrier, ACS Appl. Mater. Interfaces 2 (1) (2010) 312–320.
[20] D. Hagen, C. Box, S. Greenlee, F. Xiang, O. Regev, J. Grunlan, High gas barrier imparted by similarly charged multilayers in nanobrick wall thin films, RSC Adv. 4 (2014) 18354–18359.
[21] D. Han, Y. Luo, Q. Ju, X. Xiao, M. Xiao, N. Xiao, S. Chen, X. Peng, S. Wang, Y. Meng, Nano-brick wall architectures account for super oxygen barrier PET film by quadlayer assembly of polyelectrolytes and -ZrP nanoplatelets, Polymers 10 (2018) 1082.
[22] F. Ding, J. Liu, S. Zeng, Y. Xia, K.M. Wells, M.-P. Nieh, L. Sun, Biomimetic nanocoatings with exceptional mechanical, barrier, and flame-retardant properties from large-scale one-step coassembly, Sci. Adv. 3 (7) (2017), e1701212.
[23] A.J. Svagan, A. Åkesson, M. Cárdenas, S. Bulut, J.C. Knudsen, J. Risbo, D. Plackett, Transparent films based on PLA and montmorillonite with tunable oxygen barrier properties, Biomacromolecules 13 (2) (2012) 397–405.
[24] C. Aulin, E. Karabulut, A. Tran, L. Wågberg, T. Lindström, Transparent nanocellulosic multilayer thin films on polylactic acid with tunable gas barrier properties, ACS Appl. Mater. Interfaces 5 (15) (2013) 7352–7359.
[25] F. Carosio, S. Colonna, A. Fina, G. Rydzek, J. Hemmerlé, L. Jierry, P. Schaaf, F. Boulmedais, Efficient gas and water vapor barrier properties of thin poly(lactic acid) packaging films: functionalization with moisture resistant nafion and clay multilayers, Chem. Mater. 26 (19) (2014) 5459–5466.
[26] M.A. Priolo, D. Gamboa, K.M. Holder, J.C. Grunlan, Super gas barrier of transparent polymer-clay multilayer ultrathin films, Nano Lett. 10 (12) (2010) 4970–4974.
[27] T.T. Zhu, C.H. Zhou, F.B. Kabwe, Q.Q. Wu, C.S. Li, J.R. Zhang, Exfoliation of montmorillonite and related properties of clay/polymer nanocomposites, Appl. Clay Sci. 169 (2019) 48–66.
[28] Ramazan Asmatulu, et al., Investigating the effects of surface treatments on adhesion properties of protective coatings on carbon fiber-reinforced composite laminates, Surf. Coat. Technol. 380 (2019), 125006.
[29] A. Maattanen, P. Ihalainen, R. Bollstrom, S. Wang, M. Toivakka, J. Peltonen, Enhanced surface wetting of pigment coated paper by UVC irradiation, Ind. Eng. Chem. Res. 49 (22) (2010) 11351–11356.
[30] G. Vazquez, E. Alvarez, J.M. Navaza, Surface tension of alcohol water+ water from 20 to 50. degree. C, J. Chem. Eng. data 40 (3) (1995) 611–614.
[31] J. Nilsen-Nygaard, E.N. Fernández, T. Radusin, B.T. Rotabakk, J. Sarfraz, N. Sharmin, M.K. Pettersen, Current status of biobased and biodegradable food packaging materials: Impact on food quality and effect of innovative processing technologies, Compr. Rev. Food Sci. Food Saf. 20 (2) (2021) 1333–1380.
[32] D. Saravanan, T. Gomathi, P.N. Sudha, Sorption studies on heavy metal removal using chitin/bentonite biocomposite, Int. J. Biol. Macromol. 53 (2013) 67–71.
[33] J. Järnström, P. Ihalainen, K. Backfolk, J. Peltonen, Roughness of pigment coatings and its influence on gloss, Appl. Surf. Sci. 254 (18) (2008) 5741–5749.
[34] M.C. Krueger, B. Seiwert, A. Prager, S. Zhang, B. Abel, H. Harms, et al., Degradation of polystyrene and selected analogues by biological Fenton chemistry approaches: opportunities and limitations, Chemosphere 173 (2017) 520–528.
[35] G. Damian, F. Damian, Z. Szakács, G. Iepure, D. Aştefanei, Mineralogical and physico-chemical characterization of the oraşu-nou (romania) bentonite resources, Minerals 11 (9) (2021) 938.